

RESEARCH ARTICLE

10.1002/2014JF003294

Granulation of snow: From tumbler experiments to discrete element simulations

Walter Steinkogler^{1,2}, Johan Gaume¹, Henning Löwe¹, Betty Sovilla¹, and Michael Lehning^{1,2}¹WSL Institute for Snow and Avalanche Research SLF, Davos Dorf, Switzerland, ²CRYOS, School of Architecture, Civil and Environmental Engineering, EPFL, Lausanne, Switzerland

Key Points:

- Granulation of snow is temperature dependent
- Different granule classes can be reproduced in a concrete tumbler
- The observed granule classes can be modeled with cohesive discrete element simulations by means of aggregation and fragmentation criteria

Supporting Information:

- Figure S1
- Movie S1
- Movie S2
- Movie S3
- Movie S4
- Movie S5
- Movie S6
- Movie S7
- Movie S8

Correspondence to:

W. Steinkogler,
w.steinkogler@gmail.com

Citation:

Steinkogler, W., J. Gaume, H. Löwe, B. Sovilla, and M. Lehning (2015), Granulation of snow: From tumbler experiments to discrete element simulations, *J. Geophys. Res. Earth Surf.*, *120*, 1107–1126, doi:10.1002/2014JF003294.

Received 24 JUL 2014

Accepted 8 MAY 2015

Accepted article online 14 MAY 2015

Published online 26 JUN 2015

Abstract It is well known that snow avalanches exhibit granulation phenomena, i.e., the formation of large and apparently stable snow granules during the flow. The size distribution of the granules has an influence on flow behavior which, in turn, affects runout distances and avalanche velocities. The underlying mechanisms of granule formation are notoriously difficult to investigate within large-scale field experiments, due to limitations in the scope for measuring temperatures, velocities, and size distributions. To address this issue we present experiments with a concrete tumbler, which provide an appropriate means to investigate granule formation of snow. In a set of experiments at constant rotation velocity with varying temperatures and water content, we demonstrate that temperature has a major impact on the formation of granules. The experiments showed that granules only formed when the snow temperature exceeded -1°C . No evolution in the granule size was observed at colder temperatures. Depending on the conditions, different granulation regimes are obtained, which are qualitatively classified according to their persistence and size distribution. The potential of granulation of snow in a tumbler is further demonstrated by showing that generic features of the experiments can be reproduced by cohesive discrete element simulations. The proposed discrete element model mimics the competition between cohesive forces, which promote aggregation, and impact forces, which induce fragmentation, and supports the interpretation of the granule regime classification obtained from the tumbler experiments. Generalizations, implications for flow dynamics, and experimental and model limitations as well as suggestions for future work are discussed.

1. Introduction

Snow avalanches exhibit different flow behavior, such as a sheared and fluid-like layer, a plug flow, or a dilute suspended powder cloud [Gauer *et al.*, 2008]. Even different flow regimes can coexist at the same time at different locations inside an avalanche [Sovilla *et al.*, 2008]. The flowing dense core of an avalanche is often approximated as a granular flow [Roche *et al.*, 2011], sometimes even without taking cohesion into account [e.g., Faug *et al.*, 2009]. A comprehensive understanding of the conditions that define the particle properties and size distribution and the consequent influence on flow dynamics of avalanches are still lacking.

Recent studies have shown that the properties of the snow entrained by an avalanche during its downward motion, especially snow temperature, significantly affect flow dynamics [Naaim *et al.*, 2013; Steinkogler *et al.*, 2014a; Sovilla and Bartelt, 2002], mostly by changing the granular structure of the flow. An improved understanding of the driving factors causing the evolution of granule size distributions could help to better understand the hypermobility often observed in landslides and avalanches [Pudasaini and Miller, 2013] as well as the dynamics of powder snow avalanches [Rastello and Hopfinger, 2004].

The relation between particle size distribution and mobility of a granular flow, i.e., velocity and runout, has been emphasized in multiple studies on monodisperse and bidisperse materials [Moro *et al.*, 2010; GDR MiDi, 2004]. Investigations on particle sizes in avalanche deposits (Figure 1) were conducted [Bartelt and McArdell, 2009; De Biagi *et al.*, 2012] by collecting particles in the deposition zone of full-scale avalanches. These studies could show that wet avalanches tend to produce larger granules than dry avalanches [Bartelt and McArdell, 2009; Kobayashi *et al.*, 2000]. However, a link between different degrees of particle cohesion and emerging particle size distributions has never been quantified.

Quite generally, the dynamics of particle size distributions in cohesive flows must be understood as a competition between aggregation and fragmentation phenomena. Due to the cohesive nature of snow, pieces can aggregate upon collision and stick together to form larger units from smaller ones. Due to the impact energies



Figure 1. Granular structures in the deposition zone of an artificially released avalanche.

in a collision, pieces can also break apart and fragment into smaller ones. The competition of both processes is the origin of granulation phenomena in snow, which was so far only investigated by *Nohguchi et al.* [1997]. In the following, we refer to granulation as comprising both aggregation and fragmentation in contrast to *Walker* [2007] where the term was reserved for aggregation and enlargement of particle sizes only.

Due to the difficulties of investigating these issues within a full-scale field campaign, experiments on snow dynamics are mainly carried out in the laboratory. Most laboratory experiments are however conducted with artificial grains, e.g., glass ballotini [*Schaefer and Bugnion*, 2013], which do not take interparticle cohesion into account. Studies on wet (i.e., cohesive) granular media [*Tegzes et al.*, 2003; *Donahue et al.*, 2010] have demonstrated the impact of interstitial liquid content on the dynamic flow behavior. These findings are particularly relevant for snow avalanches where the properties and distributions of the granules are fundamental parameters influencing the flow.

An interesting experimental approach to granulation of snow is suggested by industrial applications where rotating drums are used for granulation in pharmacy [*Vervaeet and Remon*, 2005; *Kristensen and Schaefer*, 1987], ceramics processing [*Reed*, 1995], mineral processing, and fertilizer production. In these disciplines, extensive research on granulation processes [*Pietsch*, 2003] and the characterization of granule properties and size distributions has been carried out in the last decades [*Ennis et al.*, 1991; *Ouchiyaama and Tanaka*, 1975]. As an appealing side effect, granular flow in rotating drums can be well investigated by the Discrete Element Method (DEM) [*Cundall and Strack*, 1979]. A DEM approach allows to model the kinematics of a cohesive powder explicitly and predict, e.g., mixing properties in rotating drums [*Sarkar and Wassgren*, 2009, 2010; *Chaudhuri et al.*, 2006]. Numerical simulations based on DEM were also used recently to model the dense flow of cohesive granular materials by *Rognon et al.* [2008a], who studied the effect of cohesion on the flow mobility and showed that a plug region could develop if the cohesion is high enough. To our knowledge, the combination of rotating drum experiments and DEM modeling has never been used to address aggregation and fragmentation



Figure 2. Granules in motion in rotating tumbler. One of the (two) mixing blades can be seen at the lower left corner.

properties of snow for avalanche applications. It is the aim of the present paper to present a first attempt in this direction to demonstrate the potential of such a combined approach.

The paper is organized as follows. We characterize relevant snow cover parameters and parameter thresholds that control the size and properties of granules for different types of snow that formed in a rotating tumbler by ways of laboratory experiments (section 2.1) and numerical simulations (section 2.2). We then compare those results to measurements in the deposition of real-scale avalanches and suggest a diagram of the granulation regimes (section 3). We discuss our results in view of the commonly used terminology of granulation processes [Iveson *et al.*, 2001]. The paper discusses applications of the results and future avenues of research (section 4).

2. Methods

2.1. Experimental Setting

To investigate the granulation potential of different snow types, a standard, unmodified concrete tumbler (Figure 2) was used. The tumbler measures 0.6 m at the largest diameter and held 0.4 m³ of snow. The tumbler has two blades acting as mixing elements (Figure 2) and rotated with constant velocity at 0.5 rps.

All experiments were conducted in an open-door but roofed laboratory that granted easy and direct access to natural and undisturbed snow, under varying environmental conditions, i.e., different air temperatures and sunny or cloudy skies. A total of 23 experiments with varying initial snow types were conducted and resulted in measurements at 97 time steps. Snow of different types (e.g., new snow particles or melt forms) with different properties (e.g., temperature or density) was used for the experiments. To assess the initial conditions of the investigated snow (temperature, density, grain shape, grain size, moisture content, and hardness) a regular snow profile following the guidelines of Fierz *et al.* [2009] was conducted before every experiment. Consequently, snow layers with similar properties were collected and a defined volume (0.1 m³) was shoveled into the tumbler.

After defining the initial conditions of the added snow, the tumbler was started. Mellmann [2001] identified different flow regimes in rotating drums depending on the Froude number

$$Fr = \frac{\omega^2 R}{g}. \quad (1)$$

According to that analysis, our experiments should fall into the cascading regime ($Fr = 0.275$) for cohesionless particles, where the particles are transported upward through solid body rotation, with a downward surface flow of the particles (Figure 3a). However, the presence of the blades and of cohesion forced the regime into a cataracting motion, i.e., individual particles detach from the bed and were thrown off into the free space of the tumbler (Figures 2 and 3b).

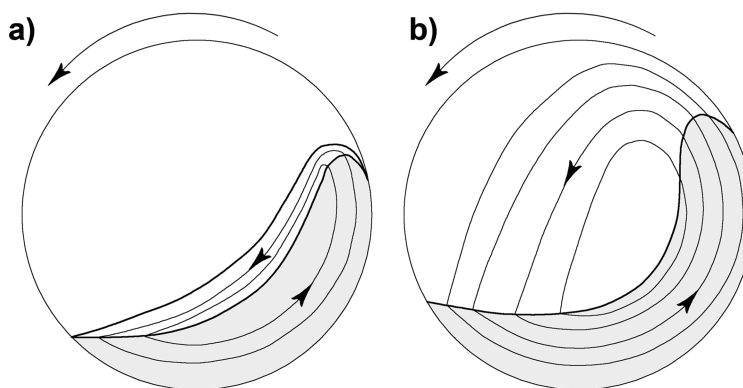


Figure 3. (a) Cascading and (b) cataracting regimes for a cohesionless granular material. These regimes mainly depend on the Froude number, particles, wall friction, and the filling degree for a cohesionless granular material (according to Mellmann [2001]).

The tumbler was stopped at regular intervals, typically every 5 min which corresponds to 150 rotations, and the properties of the snow or the formed granules were measured. Again, the same procedures and measurement devices as for standard snow profiles [Fierz *et al.*, 2009] were used. Snow temperature was measured with a digital thermometer to an accuracy of 0.1°C. Snow densities of the granules or fine material in the tumbler were measured with a 100 cm³ snow shovel and a digital scale. If the granules were too small and no sample could be taken with the density shovel, their diameter was measured and they were weighed. This was repeated for multiple granules and an average mass of sample granules was taken. Also, the liquid water content was measured following the guidelines of Fierz *et al.* [2009] by using an 8X magnification glass and squeezing the snow by hand. Grain shape and size were identified by using a crystal card and a magnifying glass.

Additionally, the experiments were filmed with normal and high-speed cameras (videos are provided as Movies S1–S8 in the supporting information). The videos reveal the motion of snow inside the tumbler and the interaction of snow and granules during collisions among themselves and with the tumbler.

We defined the initiation of granulation as soon as the snow started to form small snow balls, with a size of approximately 1 cm. If they were not hard enough to sustain collisions among themselves or were destroyed upon touching, they were defined as nonpersistent granules (Figure 4a). On the other hand, hard granules were classified as persistent. Furthermore, we distinguished between persistent-moist granules (Figure 4b), according to snow class *dry* or *moist* in Fierz *et al.* [2009], and persistent-wet granules (Figure 4c), according to *wet*, *very wet*, or *soaked* snow [Fierz *et al.*, 2009]. The experiments were continued and suspended in regular intervals until the formation of new granules could be observed. Experiments were stopped either if no granules formed after an extensive time, i.e., more than 100 min, or if the system reached a stationary state where no further changes in the measurement variables could be observed.

Measurements of the size distribution is an elaborate task in the field [Bartelt and McArdell, 2009] and in the tumbler. For our experiments we restrict ourselves to cases where granulation was visually observed and



Figure 4. Snow inside tumbler for different experiments where (a) no persistent granules formed, (b) persistent-moist granules formed, and (c) persistent-wet granules formed.



Figure 5. Small example set of different granule sizes.

characterized the full size distribution at the end of the experiment by carefully emptying the tumbler and manually evaluating the particle sizes (Figure 5).

2.2. Discrete Element Modeling

2.2.1. Motivation and Objectives

The key ingredient of granulation processes is the competition between aggregation and fragmentation of the constituents upon collisions in the flow. Aggregation and fragmentation rates thereby depend on the kinematics of the flow via collision frequencies, the mechanical properties of the particles, and particularities of the container.

Probably, the oldest approach to aggregation-fragmentation phenomena was originally suggested by *Von Smoluchowski* [1917] in the context of gelation phenomena. The model considers an evolution equation for the size distribution by providing average collision rates and size-dependent probabilities for subsequent aggregation or fragmentation events. These type of models are commonly referred to as population balance models (PBM). They must be regarded as a mean field description since expression for collision rates neither take into account spatial heterogeneities of the flow nor geometrical particularities of the container.

On the other hand, flow of granular materials can be conveniently studied within discrete element simulations to correctly capture the kinematics of the particles and spatial characteristics of forces and displacements. Thereby, collisions are taken into account explicitly and, depending on the physical insight of the aggregation and fragmentation processes, particle size distributions can be predicted including particularities of the container, such as blades in a tumbler. It is the connection of DEM and PBM [*Barrasso and Ramachandran, 2014*] which ultimately allows to upscale the processes for practical applications. DEM can be regarded as a microscopic method to predict the relevant parameters in the PBM models, which has been shown in *Reinhold and Briesen* [2012].

As a first step in this direction, we start from a cohesive granular system using the DEM by explicitly taking into account the container geometry to address the snow granulation process in a tumbler. In the DEM, a discrete element represents a “snow unit” with a size of a few millimeters. This should not be confused with a “snow grain” in the sense of *Fierz et al.* [2009], which are commonly an order of magnitude smaller. A DEM approach to tumbler experiments would require to prescribe conditions for aggregation and fragmentation of these snow units under binary collisions subject to experimental conditions of temperature and water content. A generic physical picture of these mechanical processes is almost nonexistent. We therefore start from common mechanical criteria and formulate the model in terms of aggregation and fragmentation parameters. Our choice for the parameters and the hypothesized connection to the experimental conditions will be discussed at the end.

2.2.2. Formulation of the Model

The discrete element simulations were performed using the commercial software PFC2D (by Itasca) which implements the original soft-contact algorithm described in *Cundall and Strack* [1979]. To capture the essen-

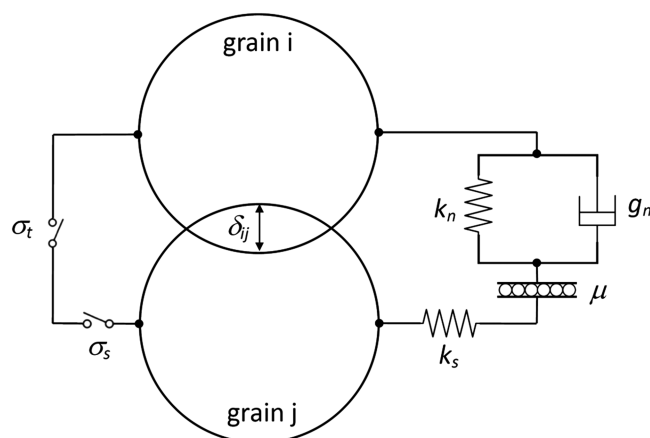


Figure 6. Schematic of the used contact law. The interpenetration distance between grain *i* and grain *j* is denoted δ_{ij} . The normal and tangential stiffnesses are denoted k_n and k_s , respectively, g_n is the viscous damping coefficient, and μ the friction coefficient. The tensile and shear strengths of the bond are denoted σ_t and σ_s .

tial details of snow granulation we carried out two-dimensional simulations of a cohesive granular material, taking into account the tumbler geometry (Figure 2). The simulated system consists of a two-dimensional outer cylinder of radius $R = 0.3$ m and blades of length $l_b = 0.35R$. This configuration corresponds to the experimental setup. The granular samples are composed of about 8000 circular particles of average diameter $d = 4.5$ mm (thus, $R/d \sim 67$), with a grain size distribution polydispersity of $\pm 30\%$ (diameters ranging from 3 to 6 mm), and a particle density $\rho_p = 300$ kg/m³.

The loading is applied by gravity and rotation of the walls (cylinder and blades). The simulations were performed in the same conditions as the experiments so as to keep the same Froude number which is equal to $Fr = 0.3$ in our case ($\omega = 3$ rad s⁻¹ and $g = 9.81$ m s⁻²). As stated before, this Froude number would correspond to a cascading regime with a cohesionless granular material (Figure 3a) [Mellmann, 2001]. However, the presence of the blades and of interparticle-particle cohesion will considerably modify and force the flow regime from the cascading to the cataracting regime (Figure 3b).

The interparticle contact laws used in the simulations are classical [Radjai et al., 2011; Gaume et al., 2011]. The normal force is the sum of a linear elastic and of a viscous contribution (spring-dashpot model), and the shear force is linear elastic with a Coulombian friction threshold (right part in Figure 6).

The corresponding mechanical parameters are summarized in Table 1. The value of the normal stiffness k_n was chosen in a way that the normal interpenetrations δ at contacts are kept small, $\delta/d < 10^{-3}$, i.e., to work in the quasi-rigid grain limit [da Cruz et al., 2005; Roux and Combe, 2002]. Concerning the normal restitution coefficient e (which is directly linked to the normal viscous damping coefficient g_n), we checked that the results presented below, and more generally all the macroscopic mechanical quantities obtained from the simulations, are actually independent of this parameter (in the range 0.1 to 0.9), in agreement with previous studies [da Cruz et al., 2005; Gaume et al., 2011; Gaume et al., 2015b].

Cohesion was added to the particles by adding a bond to each contact. This bond has specified shear and tensile strengths F_f^s and F_f^t , respectively (the subscript *f* stands for fragmentation). If the magnitude of the tensile normal contact force equals or exceeds the contact bond tensile strength, the bond breaks, and both the normal and shear contact forces are set to zero. If the magnitude of the shear contact force equals or

Table 1. Mechanical Parameters Used in the Simulations^a

k_n/P	k_n/k_s	μ	e	ρ_p	σ_t	σ_t/σ_s	F_a/F_f^t
1.10^3	2	0.5	0.1	300 kg m ⁻³	0–5 kPa	2	0–20

^a k_n : normal contact stiffness; P : average pressure; k_s : tangential contact stiffness; μ : intergranular friction; e : normal restitution coefficient; ρ_p : particle density; σ_t : contact bond tensile strength; σ_s : contact bond shear strength; F_a : bond formation force, and F_f^t : bond tensile strength (force).

exceeds the contact bond shear strength, the bond breaks, but the contact forces are not altered, provided that the shear force does not exceed the friction limit and provided that the normal force is compressive.

At the beginning of the simulation, the cohesion is applied to the whole sample. However, during the experiment, some bonds may break but new bonds may also be created at new contact points. The concept of bond formation between particles and its implementation in DEM is still open [Kroupa *et al.*, 2012]. Hence, many different bonding models currently exist and we have chosen the following simple bond formation criterion that allows us to study the competing effects of fragmentation and aggregation of bonds:

$$\sqrt{N_{ij}^2 + S_{ij}^2} > F_a \quad (2)$$

where F_a is the bond formation force (the subscript a stands for aggregation), N_{ij} and S_{ij} the normal and shear forces at the contact, respectively. A similar model was already implemented in Brown [2013], Patwa *et al.* [2014], and Boltachev *et al.* [2014] with a creation criterion based on the exceedance of a critical interpenetration distance. This criterion is equivalent to our force criterion as the force is a linear function of interpenetration. Furthermore, Siirä *et al.* [2011] also used the same force threshold criterion for bond formation to study powder tableting.

The contact law which is used in the model is summarized schematically in Figure 6 in which the viscoelastic part is on the right side and the cohesive (plastic) part on the left side, and the ranges of the used parameters are shown in Table 1.

Different models of cohesive interaction could also have been used such as the cohesive potential model of Rognon *et al.* [2008b] (attractive force for short interpenetrations between the grains followed by repulsive force for higher interpenetrations). However, due to the complexity of snow, it would have been difficult, in practice, to link the parameters of this model to snow properties. Our model is simpler and also more straightforward to apply to snow. Its model parameters, namely, the tensile strength [Hagenmüller *et al.*, 2014; Sigrist, 2006] and the bond formation force [Podolskiy *et al.*, 2014; Szabo and Schneebeli, 2007], can be evaluated from laboratory experiments.

2.2.3. Dimensional Analysis

Snow is a material generally characterized in terms of stresses rather than forces. Hence, the tensile and shear strengths F_f^t and F_f^s (forces) are scaled by the bond surface to obtain the tensile and shear strengths σ^t and σ^s (stresses):

$$\sigma^t = \frac{4 F_f^t}{\pi d^2} \quad \text{and} \quad \sigma^s = \frac{4 F_f^s}{\pi d^2} \quad (3)$$

Realistic values of the tensile and shear strengths for cohesive snow can be found in the literature [Mellor, 1974; Jamieson and Johnston, 1990, 2001; Gaume *et al.*, 2012, 2015a] and belong to the range 0–5 kPa.

Furthermore, following Rognon *et al.* [2008b], different dimensionless numbers are used to quantify the intensity of the interparticle strength. These numbers compare the contact bond tensile strength F_f^t and the bond formation force F_a to two typical forces of the system. The first number η_f (fragmentation number) characterizes the fragmentation potential of a bond after a collision due to the cataracting regime of the tumbler:

$$\eta_f = \frac{\sqrt{m_p k_n \langle v \rangle}}{F_f^t}, \quad (4)$$

where m_p is the particle mass and $\langle v \rangle = \langle R_p \rangle \omega$ the average particle velocity ($\langle R_p \rangle$ is the average particle radial position). The fragmentation number thus compares F_f^t to the impact force of an elastic body. This number is nevertheless different from that used in Rognon *et al.* [2008b] for a gravitational shear flow which compares F_f^t to the gravitational force mg . In our case, the main source of granule breakage are granule collisions, so our fragmentation number was modified accordingly.

The second number η_a (aggregation number) characterizes the potential of formation of a new bond inside a granular assembly submitted to a pressure P

$$\eta_a = \frac{Pd^2}{F_a}. \quad (5)$$

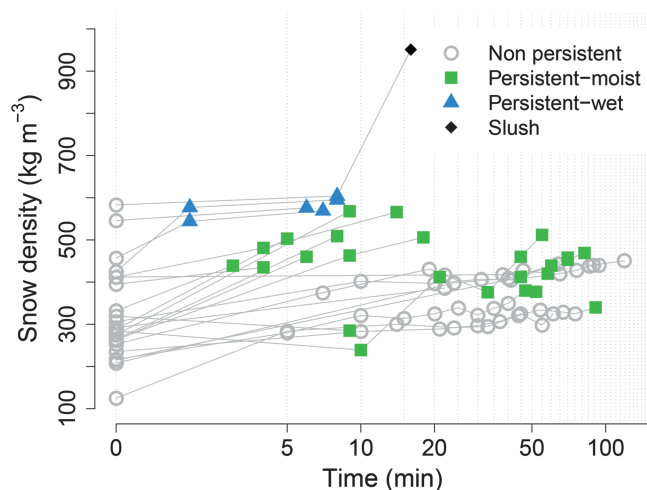


Figure 7. Snow density measurements (bulk density from 100 cm³ shovel) for all individual experiments (gray lines) and time of each measurement (gray and colored markers) for persistent-moist (colored squares) and persistent-wet (colored triangles) granules.

This number compares F_a to the average normal force Pd^2 due to pressure. According to this definition and to Rognon *et al.* [2008b], a transition between different cohesive flow regimes should depend on these two numbers η_f and η_a and should occur for values close to unity. In our study, F_f^t was varied between 0 and 0.05 N and F_a between 0 and 1 N. The collisional force is equal to $\sqrt{m_p k_n v} \approx 0.023$ N ($\langle R_p \rangle \approx 0.2$) and the average pressure force is equal to $Pd^2 \approx 0.018$ N by taking $P = \rho g R$, the hydrostatic pressure at the bottom of the tumbler. The fragmentation number η_f typically varies in the range 0.5–4.5 and the aggregation number η_a in the range 0.01–10.

2.2.4. Simulation Procedure and Granule Definition

Simulations were performed for 6 different values of F_f^t and 15 of F_a (and thus different values of η_f and η_a) for a total of 90 simulations. At the beginning of each simulation, cohesion is applied to the whole sample so it forms a single large block similar to a cohesive slab in the release zone of an avalanche. The simulations were stopped after 30 revolutions, corresponding to an apparent steady state (almost constant size distribution).

At each quarter revolution, the granules are identified as a cluster of particles linked by cohesive bonds and the size of these different clusters was computed. The procedure of cluster identification is provided as supporting information. As the granules may not be perfectly circular, the maximum transverse length was retained, similar to what was measured experimentally. Hence, for each simulation, the complete granules size distribution was available as a function of time. In addition to the granules size, the average number of cohesive bonds per granule was computed.

3. Results

In this section we discuss the measured snow cover parameters and their temporal evolution during the experiments and identify the most relevant parameters for the granulation process (section 3.1). Depending on the persistence of the formed granules, all conducted experiments are assigned to three granulation classes. This classification also provides the basis for the DEM simulations which supplement the measurements (section 3.2). We summarize the main results of experiments and modeling in Figure 15 and finally present a combined view of experimental, modeled, and real-scale avalanche size distributions (section 3.3).

3.1. Evolution of Snow Parameters

The following graphs (Figures 7 to 12) display all individual experiments (gray lines), the time of each measurement (gray and colored markers), and whether nonpersistent (gray circles), persistent-moist (colored squares), or persistent-wet (colored triangles) granules were recorded.

Most experiments were initialized with a snow density between 200 and 350 kg m⁻³ (Figure 7). Densities of persistent granules reached similar values as observed in the deposition of real-scale avalanches (400 kg m⁻³).

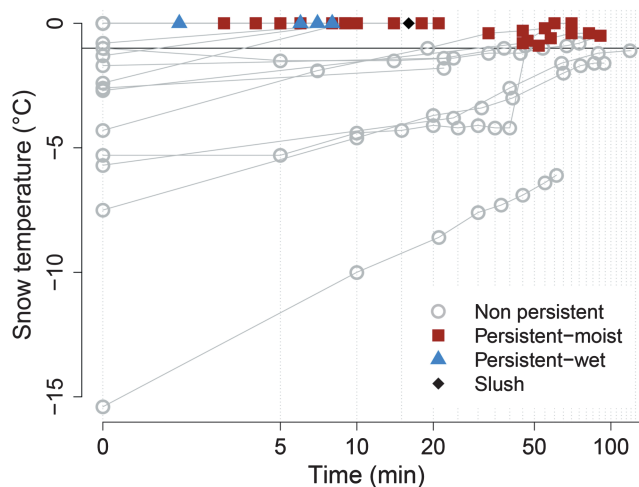


Figure 8. Snow temperature measurements for all individual experiments (gray lines) and time of each measurement (gray and colored markers) for persistent-moist (colored squares) and persistent-wet (colored triangles) granules.

Densities larger than 550 kg m^{-3} were only observed for persistent-wet granules. For the slush experiment (snow density of 951 kg m^{-3}) water was added after persistent-wet granules had formed. In many experiments with no persistent granulation, the density of the remaining fine, ungranulated snow also reached values up to 450 kg m^{-3} . The error for the snow density measurements was around $\pm 10 \text{ kg m}^{-3}$.

A strong dependency of granulation on snow temperature could be observed (Figure 8). Once a temperature of -1°C was reached, granulation occurred very fast (colored markers in Figure 8). Multiple experiments below the threshold of -1°C were run for an extensive duration (more than 100 min), yet no persistent granules could be observed (gray circles in Figure 8). The measurement error was in the range of the accuracy of the used thermometer (0.1°C).

Following the classification of *Fierz et al. [2009]*, water could neither be recognized by eye nor by magnification for persistent-moist granules yet the snow showed a distinct tendency to stick together (Figure 9). Liquid water was only observed for persistent-wet granules. Most experiments with nonpersistent granules could be observed for dry snow conditions. Even though many persistent-moist experiments were at or close to 0°C , they never reached the wet class. Persistent-wet granulation only occurred if the initial snow was already wet or water was added to the tumbler.

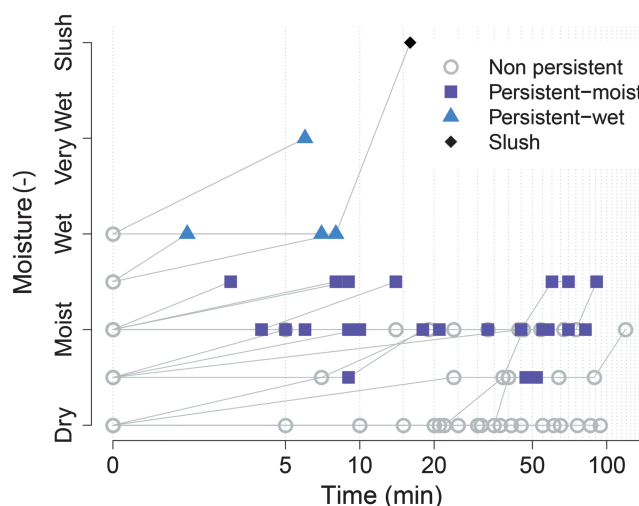


Figure 9. Snow moisture measurements for all individual experiments (gray lines) and time of each measurement (gray and colored markers) for persistent-moist (colored squares) and persistent-wet (colored triangles) granules.

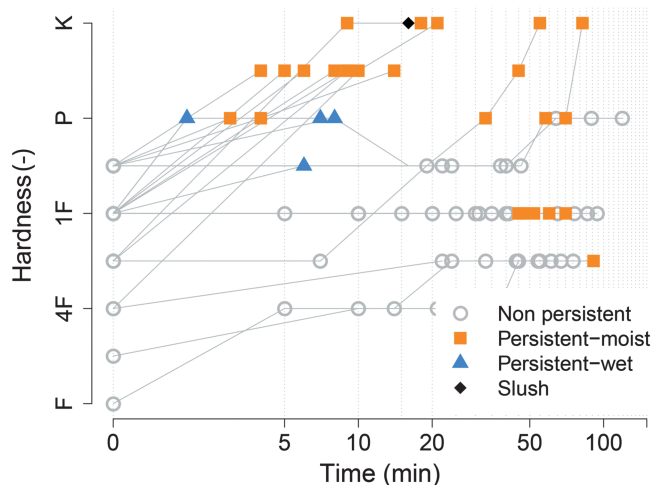


Figure 10. Hardness measurements for all individual experiments (gray lines) and time of each measurement (gray and colored markers) for persistent-moist (colored squares) and persistent-wet (colored triangles) granules.

For most experiments with persistent granules, the hardness (Figure 10) increased to *pencil* or *knife* [Fierz et al., 2009] in a short time and the granules did not break apart anymore at this stage upon collision inside the tumbler. In many cases persistent-wet granules were softer than persistent-moist granules. Less hard granules usually were not persistent and got destroyed by consequent rotations of the tumbler (see videos in the supporting information).

No distinct correlation between grain size and granulation potential could be observed (Figure 11). Generally, no large variations in grain size during the experiments could be observed. Persistent-wet granules showed larger grain sizes since the initial snow in those cases contained mostly large melt forms.

Persistent-wet granules were only observed when melt forms were used as initial snow (Figure 12). No significant rounding or changing to melt forms due to friction of crystals could be observed. Decomposed forms that were rapidly mechanically transformed to rounded grains were most efficient to create persistent-moist granules. However, melt forms also resulted in persistent-moist granules in some cases.

Out of all conducted tumbler experiments, four experiments developed no persistent granules (Figure 4a); in 15 experiments, persistent-moist granules formed (Figure 4b); and in three experiments, persistent-wet granules were observed (Figure 4c). For one experiment, liquid water was added to the tumbler to create a

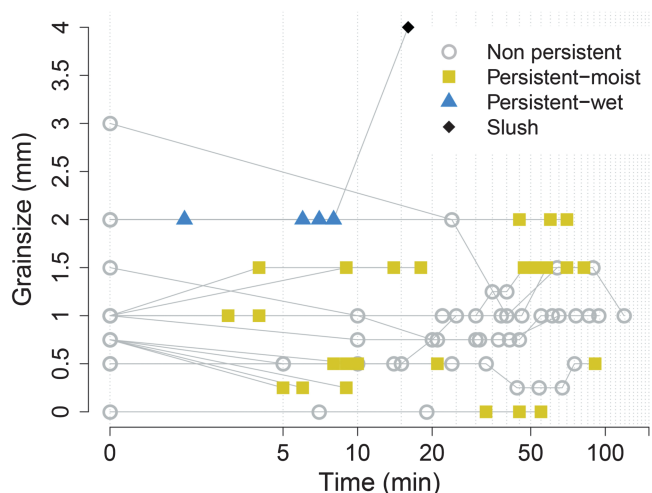


Figure 11. Grain size measurements for all individual experiments (gray lines) and time of each measurement (gray and colored markers) for persistent-moist (colored squares) and persistent-wet (colored triangles) granules.

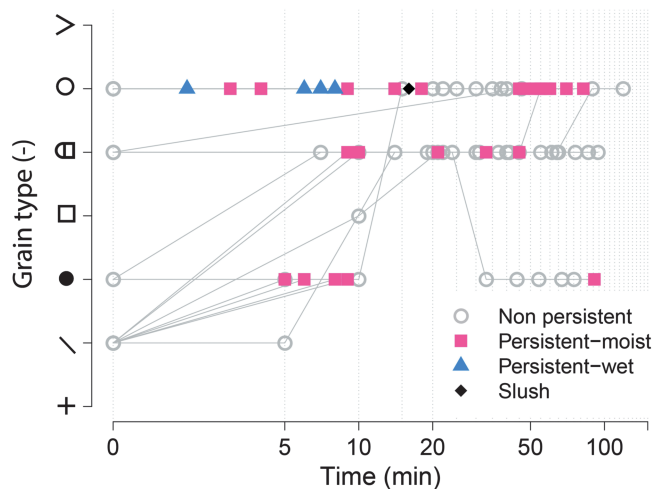


Figure 12. Grain type measurements for all individual experiments (gray lines) and time of each measurement (gray and colored markers) for persistent-moist (colored squares) and persistent-wet (colored triangles) granules.

slushy flow. The snow or granules that formed inside the tumbler are classified depending on their properties and snow cover parameters.

The granulation process for persistent-moist granules was observed to take place in two stages. As soon as the temperature threshold of -1°C was reached, individual granules (Figure 13a) were observed to grow until a size of approximately 1 to 4 cm. For most experiments, these initial granules also rapidly densified (Figure 7) and increased in hardness (Figure 10). In a second stage, these individual granules started to form larger aggregates (Figure 13b). At the final stage of granulation for moist experiments, a mixture of individual granules, aggregates, and leftover fine material existed inside the tumbler.

3.2. Numerical Results

The conducted DEM simulations allow to discuss the different observed granulation classes and relevant snow parameters (section 3.1) in more detail with respect to the determining physical processes, i.e., aggregation and fragmentation.

Figure 14 represents the average granule radius $\langle r_g \rangle$ as a function of the two dimensionless numbers η_a and η_f at the end of the simulation. The range of simulations allowed to observe average granule radii ranging from almost zero (the particle radius $r_p = 2.25 \times 10^{-3}$ mm) to the radius of the tumbler ($R = 30$ cm) corresponding to one single large granule.

If the aggregation number η_a is low, typically lower than 0.2, then only the fragmentation number has an influence on the granules size distribution. In this case, the force required to create a new bond is too high compared to the force due to pressure. Hence, the only possible process is the breakage of the existing bonds due to possible dynamic collisions. In this regime ($\eta_a < 0.2$) and for $\eta_f > 1$ (zone A) the average granule radius

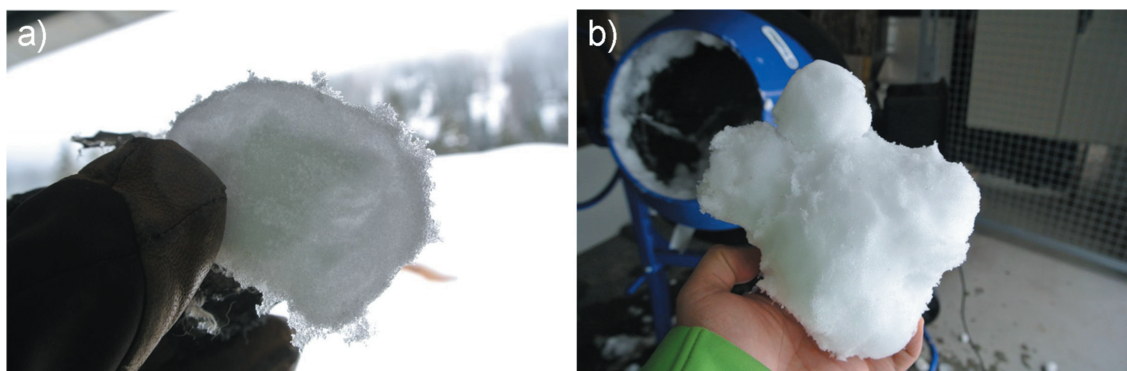


Figure 13. (a) Persistent-moist granules at a very initial stage and (b) aggregates of multiple individual granules at the end of the experiment.

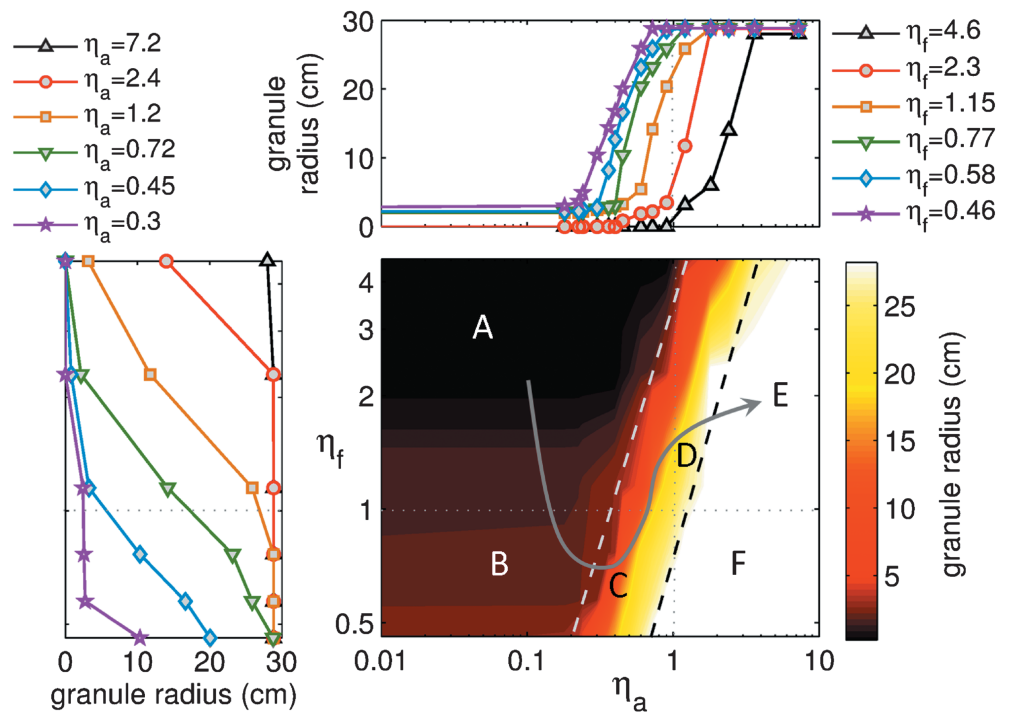


Figure 14. Contour plot of the granule radius as a function of (top right) aggregation number η_a and (left) fragmentation number η_f showing the different granulation regimes. Zone A: No granules, zone B: granules due to breakage, zone C: persistent-moist granules, zone D: persistent-wet granules, zone E: slush (or pasty flow), and zone F: one large granule. The domain between the dashed lines corresponds to $0.75 < \eta_a/\eta_f < 3$. The gray curved arrow represents a qualitative path for the evolution of the breakage and formation numbers with increasing snow temperature and liquid water content.

$\langle r_g \rangle$ is approximately equal to the particle radius r_p . The bond strength is then not high enough to resist the dynamic collisions imposed by the system and thus no granules persist. If the bond strength increases so that the fragmentation number η_f becomes smaller than 1 (zone B), then some more persistent granules appear. The average granule radius therefore increases with increasing strength. Note also that for $\eta_f \ll 0.5$ (not represented on the diagram), the cohesive bonds never break leading to one single and large granule whose radius is a little bit lower than the tumbler radius ($r_g \approx 28$ cm).

For $\eta_a > 0.2$, the evolution of the average granule size with η_a and η_f becomes more complex. For constant values of the bond strength, the average granule radius $\langle r_g \rangle$ increases with increasing aggregation number η_a (Figure 14, top right) up to the tumbler radius. The rate of change of $\langle r_g \rangle$ with η_a is almost independent of η_f . The average granule size strongly depends on the fragmentation number η_f , lower values corresponding to lower granule sizes (Figure 14, left). Hence, for $\eta_a > 0.2$ a competition between bond creation and breakage determines the average granules size. Inside the zones delimited by dashed lines (corresponding to $0.75 < \eta_f/\eta_a < 3$, zones C and D) on Figure 14, the average granule size is a linear function of the ratio between the fragmentation number and the aggregation number:

$$\langle r_g \rangle \approx 20.5 \left(\frac{\eta_a}{\eta_f} \right)^{4/3} \tag{6}$$

If $\eta_a/\eta_f < 0.75$ then the average granule radius depends only on the fragmentation number as detailed before. The difference between zones C and D is therefore linked to the strength of the granules, stronger in C and weaker in D but leading to the same granule sizes. On the other hand, if $\eta_f/\eta_a > 3$ then the average granule radius is equal to the tumbler radius which is the limiting size of the system. Hence, zone F corresponds to a regime with a unique strong (low fragmentation number) and large granule whereas zone E corresponds to a pasty-like flow regime in which new bonds are created at each contact point every time step but whose strength is very small.

In addition, the average number of bonds per particle inside a granule was also recorded and changed with regard to the aggregation and fragmentation numbers. For high fragmentation η_f and low aggregation η_a



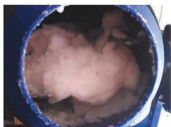

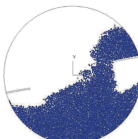



Experiments:				
				
Granule persistence	non persistent	persistent	persistent	non persistent
Snow temperature	$< -1^{\circ}C$	$> -1^{\circ}C$	$0^{\circ}C$	$0^{\circ}C$
Moisture content	dry	moist	wet	very wet or slush
Temperature class	cold	warm	warm	warm
Granule/Particle size	crystal scale (mm)	$\sim 2-10$ cm	$\sim 10-25$ cm	-
Mode of failure	brittle (fragmentation)	quasi-brittle	ductile	pasty/viscous
Collision type	destructive	elastic	plastic	-
DEM:				
				
Flow type	cohesionless granular	granular	granular / viscous	pasty / viscous
Fragmentation number	>1	<1	>1	>1
Aggregation number	<0.5	$0.2-1$	≈ 1	>2

Figure 15. Summary of experiments and discrete element simulations.

numbers (zone A), the average number of bond per particle is close to zero. For low fragmentation and aggregation numbers (zone B), the average number of bonds per particle is around 2.7. In zone F (high aggregation and low fragmentation), the average number of bonds per particle is around 4.6 whereas it is around 2.9 in zone E (high aggregation and high fragmentation).

The model results were added to the experimentally defined granulation classes in Figure 15. Videos of the simulations are provided as supporting information for the four main granulation regimes (nonpersistent, persistent-moist, persistent-wet, and slush).

3.3. Granule Size Distribution

Eventually, a stationary state is reached where there is a balance between collisions, which fragment particles and those which aggregate particles [Walker, 2007; Kapur, 1971]. At this point, a stable granule size distribution is attained.

Figure 16 compares the granule size distributions for two tumbler experiments, persistent-moist (violet filled circles) and persistent-wet (green filled squares), the corresponding DEM simulations (violet and green lines) and a distribution as observed in avalanche deposits (blue triangles) (see Steinkogler et al. [2014b], for more information on the real-scale avalanches). Note that for the sake of the comparison with experiments, the lowest values of granule sizes were excluded to compute the size distribution. Indeed, experimentally, the very fine particles could not be measured. Hence, for size distributions obtained through the DEM, only granule sizes larger than the smallest size observed experimentally were retained explaining the sharp tail in Figure 16.

The granule size showed a typical log-normal distribution [Bartelt and McArdell, 2009], although with a shift toward smaller granule sizes compared to real-scale avalanches and the DEM results are in good agreement with the measurements.

4. Discussion

The presented approach (summary in Figure 15) suggests that granulation, as observed in natural avalanches, can be reproduced and studied within concrete tumbler experiments and cohesive discrete element modeling. In the following, we first recap the main results (section 4.1) and discuss the aggregation process in respect of dry (section 4.2) and wet cohesion (section 4.3). We then provide an interpretation of the observed granule classes by combining experimental and modeling findings (section 4.4). Finally, the limitations of our experimental and model setup are addressed (section 4.5) and we turn to the application of our results and discuss possible implications for flow dynamics (section 4.6).

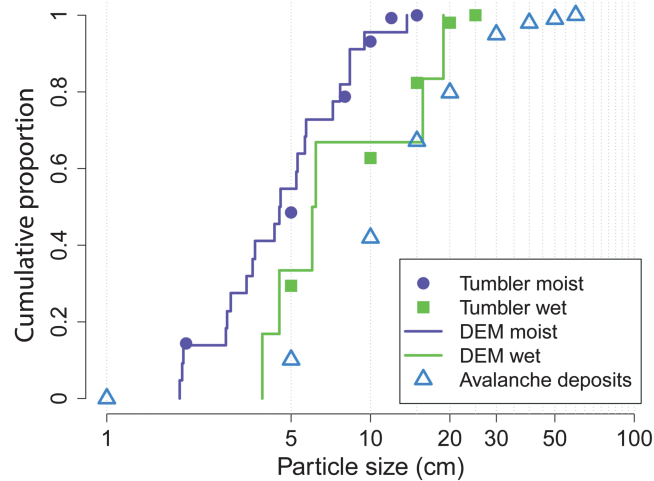


Figure 16. Granule size distributions conducted for selected tumbler experiments, persistent-moist (violet filled circles) and persistent-wet (green filled squares), DEM simulations (violet and green lines), and in the deposition area of an artificially released avalanche (blue triangles). The “moist” DEM simulation corresponds to $\eta_f = 0.5$ and $\eta_a = 0.3$, while the wet DEM simulation corresponds to $\eta_f = 1.15$ and $\eta_a = 0.8$.

The general mechanisms underlying the snow granulation process are well described in literature for other examples [Iveson *et al.*, 2001; Hapgood *et al.*, 2007]. From the initial ensemble of constituent snow “particles,” larger granules form and grow due to the presence of cohesive forces between the particles. The original, fine-grained snow (Figure 13a) aggregates upon collision of two or multiple granules which stick together to form a single large granule (Figure 13b). Once formed, granules may consolidate during the collision by mechanical compaction or may likewise fragment again if the overall strength of the granule is too small. Overall, the emergence, stability, and size characteristics of the granule system is the result of a competition between aggregation and fragmentation of snow particles upon collision.

4.1. Main Results

As a main experimental result we found that the emergence of granules occurs above a distinct temperature threshold of -1°C (Figure 8). Once this threshold was reached we observed an abrupt change and a transition from nonpersistent to persistent granule types (Figure 15) while all other measured snow parameters, like density and hardness, evolve in a continuous, monotonic manner. Although the densities are similar for all cases (Figure 7), our results show that granules vary in strength which is used as a main classification criterion (Figure 15).

The high-speed videos (supporting information) allow for a qualitative interpretation of the strength of the granules and are in agreement with multiple studies on breakage patterns of aggregates [Mishra and Thornton, 2001]. The videos show that the granules are lifted and consequently collide with the outer wall of the tumbler, other granules, or the blades after falling the entire diameter of the tumbler. Granule strengths ranged from soft and nonpersistent, which fractured upon touching or particle collisions, to very hard and persistent granules which even resisted the impact on the sharp side of the blades inside the tumbler. Nonpersistent granules were usually destroyed and completely fragmented at every rotation of the tumbler. For persistent-moist granules a localized disintegration [Subero and Ghadiri, 2001], i.e., the damage is restricted to the impact area, was observed. Those granules were only destroyed if they were dropped from 1 to 2 m on the concrete floor. In those cases they showed a semi-brittle behavior [Cheong *et al.*, 2005], i.e., the fracture is preceded by limited plastic deformation. Persistent-wet granules showed a ductile behavior. This indicates a very different energy dissipation depending on the granule type.

From a modeling perspective, we have set up a DEM and solely varied the probability of establishing a cohesive bond (aggregation) and the strength of these (fragmentation) (Figure 14). In the following we will address the expected role of temperature on the physical interactions in the real system and their translation to the parameters of the DEM approach. Given a threshold of -1°C and the additional introduction of water in some cases, we are dealing with both types of forces, dry cohesive forces which are mediated by fast sintering processes [Szabo and Schneebeli, 2007] and wet cohesive forces mediated by the presence of liquid bridges and capillary effects [Mitarai and Nori, 2006].

4.2. Dry Cohesion

For dry cohesion, fast sintering processes [Szabo and Schneebeli, 2007] are known to be temperature dependent [Casassa *et al.*, 1991]. The “pull-off” force of an ice-ice contact after a certain contact time shows a monotonic increase with temperature. For dry cohesion alone, a temperature increase can be directly translated to a strong increase of the aggregation number and a decrease of the fragmentation number in the simulations. Sintering becomes particularly fast, close to the melting point, potentially due to the onset of surface melting and the emergence of a quasi-liquid layer [Dash *et al.*, 2006]. We also observe a pronounced effect and the most distinct persistent-moist granulation close to 0°C.

Concerning fragmentation in the dry case, Subero and Ghadiri [2001] noted that the fracture of aggregates (Figure 13b) is more complicated than that of their homogeneous counterpart. The fracture of homogeneous snow is yet not fully understood [Sigrist *et al.*, 2005]. For aggregates, the strength is expected to depend on the bonding mechanism as discussed by Mishra and Thornton [2001]. Indeed, the densification during tumbler rotation (Figure 7) plays a role, since fracture toughness of snow depends on density [McClung, 2009; Bazant *et al.*, 2003]. Hapgood *et al.* [2007] observed that the extent of consolidation depends on the intensity of agitation in the tumbler and resistance of the granule to deformation. This can also be observed in our experiments as snow that was initially soft, e.g., hardness class *one finger*, granulated into consolidated granules with a hardness of *knife* (Figure 10) and also rapidly densified (Figure 7). The increase of temperature should tend to shift the mechanical behavior of the aggregates from brittle to ductile. The rate of the deformations should be controlled by the typical velocities of the particles. Typical velocities are, in turn, controlled by the tumbler frequency which is left constant in the present approach.

4.3. Wet Cohesion

Effects of dry cohesion might be masked by capillary effects close to the melting point. As soon as the snow temperature reaches 0°C, the amount of liquid water clearly dominates the formation and properties of the granules. Note that we only measured liquid water content by traditional methods (Figure 9). Since the system is not in thermal equilibrium, it is possible that small amounts of liquid water are present which are not detected. Thus, capillary effects may become important. In particular, for the class of persistent-wet granulation (Figure 15), the presence of liquid water and capillary forces plays an important role. For the wet case, the temperature dependence of the cohesion is different from the dry case. The attractive force of a single capillary bridge of liquid water will hardly be influenced by temperature, since the relevant parameter, namely, the surface energy of water, shows only a weak temperature dependence in that regime [Pruppacher and Klett, 1997]. However, the temperature influences the *amount* of liquid water and thus the number of capillary bonds. The snow granules then display the mechanical stability of a wet granular assembly, which is a nonmonotonic function of water content [Mitarai and Nori, 2006, and references therein]. Initially, the strength increases with increasing water content and then sharply decreases. If the material becomes fully saturated, the strength vanishes. Only the presence of small amounts of a wetting liquid, which is the case for our persistent-wet regime, can dramatically change granule properties [Hornbaker *et al.*, 1997; Schiffer, 2005; Nowak *et al.*, 2005; Mitarai and Nori, 2006].

4.4. Link Between Experiments and DEM Simulations

The DEM contains two different dimensionless parameters, the aggregation and fragmentation number (section 2.2), which mimic the main physical effects of temperature and liquid water content on the granulation. A new bond is created and two particles aggregate to a cluster, if the contact force between two particles exceeds a threshold. This is controlled by the aggregation number. On the other hand, if the normal (or shear) force exceeds the bond tensile (or shear) strength, the bond does not persist and the granule will fragment. As a consequence, we find that the experimentally observed granule classes (Figure 15) can be represented by a “phase diagram” (Figure 14).

4.4.1. Nonpersistent Granules (Zone A)

In the experiment the snow was always below -1°C and dry, and the formed nonpersistent granules easily broke upon collisions. This resulted in a cohesionless granular flow inside the tumbler. The DEM simulations reproduced this behavior in zone A (Figure 14) where the formation of new bonds was not very likely, i.e., an aggregation number $\eta_a < 0.5$ and the bond strength was too small to sustain the collisions imposed by the system, i.e., fragmentation number $\eta_f > 1$.

In zone B granules were only the result of a breakage process ($\eta_f > 1$ and $\eta_a > 0.5$) which was not observed in the tumbler experiments since in those cases the snow was already fragmented by the process of shoveling

into the tumbler. Yet this is similar to observations in dry, cold avalanches where granular structures in the deposits are remaining parts of the slab and the eroded snow cover.

4.4.2. Persistent-Moist Granules (Zone C)

As soon as the temperature threshold of -1°C was reached and the snow was observed to be dry to moist, hard granules formed which even resisted direct impacts on the mixing blades (see Movies S2 and S6). Szabo and Schneebeli [2007] noted that the impact between two ice particles can cause the temporary melting of the interfacial region, thus possibly explaining the threshold for granulation to be already at -1°C . The DEM simulations (Figure 14) indicated that the fragmentation number η_f needed to be smaller than 1, i.e., the granules resist most collisions, and the aggregation number η_a was between 0.2 and 1, i.e., allowing a slight growth, to ultimately facilitate the formation of persistent-moist granules (zone C). It is worth noting that the measured maximum snow densities, around $450\text{ kg}\cdot\text{m}^{-3}$, were very similar to the ones observed in the deposition area of real-scale avalanches [Sovilla et al., 2007]. This indicates that the formation of granules in general and the observed maximum densities were defined by the snow properties itself and not due to pressure or forces inside an avalanche.

4.4.3. Persistent-Wet Granules (Zone D)

As the snow reached 0°C and was observed to be wet to very wet the formed granules were softer and deformed or broke upon impacts. The snow had a clear tendency to stick together, but the formed granules often broke apart again. To obtain a persistent-wet granulation regime (zone D) with the DEM simulations, the fragmentation number η_f needed to be higher than 1, i.e., breakage through collisions occurred but due to the large aggregation number (η_a around 1) new bonds were easily formed, ensuring large granule sizes but at a lower strength than for persistent-moist granules (zone C).

4.4.4. Slush (Zone E)

The snow was at 0°C and saturated with water. Instead of granules a pasty-like (viscous) flow was observed. In this case the aggregation number was very large, $\eta_a > 2$, causing the particles to bond almost at every time step. However, the fragmentation number being also large, $\eta_f > 1$, these bonds immediately break again leading to complex interactions and the observed pasty-like flow.

Upon temperature increase and the associated increase of liquid water content, we expect to transit from a cold and dry regime (zones A and B), to a persistent-moist regime with a maximum granule strength (zone C), to a persistent-wet regime (zone D), and finally to a slushy and water saturated regime (zone E) with a very low strength. This should correspond to a path in parameter space which is qualitatively represented by the gray line in Figure 14. The abrupt transition from nonpersistent to persistent granules observed in the experiments at a certain temperature should roughly correspond to the sharp transition on that path when crossing the phase boundary in $\eta_a - \eta_f$ parameter space.

The geometry of the tumbler with the blades seem to be an unnecessary complication for the DEM approach, which is clearly absent in real avalanches. The blades are required to promote granular mixing. The inclusion of the geometry in the simulation is facilitated by the dimensional analysis of the DEM (section 2.2) which allows to simulate realistic parameter regimes, even by explicitly including the geometry and blades in the tumbler. This enables a direct comparison of the simulation with the experiments. Even though some relevant, qualitative features of the granulation process are well captured by the DEM, some experimental and model limitations must be acknowledged.

4.5. Limitations of Experimental and Modeling Setup

One of the main shortcomings of the experimental setup is the limited control of heat supply to the system. This prevents us to detect a potential temperature increase by internal friction. An improved experimental setup should envisage thermal insulation of the tumbler, potentially with a controlled heat flux to vary the temperature. Thereby, a temperature analysis should be able to indicate effects from internal heating. When approaching 0°C , precise measurements of the liquid water content will be important to discern effects of liquid and dry cohesion in the granular system. An additional helpful modification of the tumbler would be a less "singular" geometry of the mixing elements to avoid the cutting impact of the blades on the granules.

While our experiments have thus far provided a broad overview about the influence of various quantities, future experiments should focus on dedicated parameter studies. A crucial parameter which could be easily varied is the tumbler frequency which influences collision rates, contact times and breakage probabilities.

To further constrain the parameters of the model, the viscoelastic properties of the granules and the strength of the bonds need to be known. A large body of experimental work on the static strength of liquid-bound

granules [Iveson *et al.*, 2001] already exists. These have been measured either by direct tensile tests or uniaxial compression tests where the granule is assumed to fail due to tensile stress. Also, the mechanical response of aggregates at high and low strain rates [Cheong *et al.*, 2005] has not been investigated yet. Schubert [1977] has described the different methods available to measure the strength of moist aggregates. There are two main parameters of interest that are usually reported: peak yield stress and the maximum strain before brittle failure. At least bounds on mechanical properties could be easily obtained by including mechanical tests of the snow before and after granule formation at the beginning and end of the experiment [Scapozza and Bartelt, 2003].

On the modeling side, the process of granule growth in the simulation always starts from aggregating constituent particles. The initial particles with size ($d = 4.5$ mm) must be already regarded as small granules (Figure 13). Using smaller sizes of < 1 mm, similar to realistic snow grains, would however require considerable computational effort. So the effect of using different initial conditions in the simulation remains to be addressed in the future. Furthermore, the time and pressure dependence of the sintering force and the strength as observed in Szabo and Schneebeli [2007] and Podolskiy *et al.* [2014] which might induce compaction effects are not accounted for in our model but might affect the persistency and the strength of the granules due to progressive consolidation. However, densification and compaction effects are observed in the model results as highlighted (see section 3.2) by the increasing number of bonds per particle inside a granule [Louge *et al.*, 2011] with increasing aggregation and decreasing fragmentation numbers.

Being aware of the present limitations of the approach, the observed differences in the properties of non-persistent and persistent granules are of relevance for flow dynamics since the macroscopic behavior of a granular material is determined by the nature of the interactions between the grains [Andreotti *et al.*, 2013].

4.6. Implications for Flow Dynamics

Granulation can influence flow dynamics in two possible ways: by changing the size distribution of the flowing particles [Pouliquen, 1999] and by a change of their properties [Rognon *et al.*, 2008a; Alexander *et al.*, 2006].

Multiple studies [Moro *et al.*, 2010; Phillips *et al.*, 2006; Andreotti *et al.*, 2013] show that the size distribution can fundamentally affect the flow dynamics. Our results show that the granule size distribution is determined by snow cover properties. For avalanches consisting of cold snow, i.e., $< -1^{\circ}\text{C}$, a fine-grained structure with non-persistent granules can be expected. Even though granular structures are often observed in the deposit of avalanches in this temperature range [Bartelt and McArdell, 2009], these granules are likely to be fragments of the released or eroded snow cover (Figure 1). Furthermore, these observations are only performed on top of the surface of the deposits and only represent 10–20% of the overall flowing mass.

On the contrary, we expect that avalanches consisting of warm snow, i.e., $> -1^{\circ}\text{C}$ and possibly containing liquid water, to consist entirely of persistent granules. Kobayashi *et al.* [2000] noted that the particle size distribution of snowballs in dry granulation was wider than that in wet agglomeration. This was also found in our study, since both tumbler experiments and DEM simulations showed fewer but much larger granules for persistent-wet experiments than for persistent-moist granules. Further, our results also suggest that in real-scale avalanches segregation processes and the resulting levée/channel morphology [Bartelt *et al.*, 2012] in the deposition zone are processes which are mostly relevant for avalanches where the snow temperature is above -1°C .

The properties of the granules also significantly influence flow dynamics and define the flow regime of avalanches, e.g., whether a plug or a sheared flow forms. In real-scale avalanches, these two flow regimes are found in warm and cold avalanches, respectively [Kern *et al.*, 2010; Sovilla *et al.*, 2008]. Full-scale warm snow avalanches measured at the Vallée de la Sionne field site in the Western Swiss Alps [Sovilla *et al.*, 2008] are characterized by plug flow of several meters in depth and slide over a thin basal layer of snow grains. Our experiments suggest that the large values of cohesion and sintering acting inside and between granules when the snow temperature exceeds -1°C enhance the resistance of particle to shear in analogy to granular experiments by Rognon *et al.* [2008a]. In contrast, dry and cold avalanches, which are expected to consist of nonpersistent granules, fine grains without cohesion, and/or remaining fragments of the released and eroded snow cover, typically develop a sheared flow.

Moreover, the different granular structures between wet and dry-snow dense avalanches may also explain the significantly different pressures measured in the two flow typologies [Sovilla *et al.*, 2010; Baroudi *et al.*, 2011]. Recently, it has been postulated that the pressure exerted by a wet-snow avalanche can be attributed to the

formation and collapse of force-chain structures forming when the avalanche interact against an obstacle. Our results indicate that these chains seem to be more developed and persistent when the snow temperature rises above -1°C and persistent granules form.

5. Conclusions

The granular properties, i.e., the size distribution and mechanical properties, significantly influence the flow dynamics of avalanches. It is therefore necessary to identify the determining factors which define the granulation process of snow. In this study we present a simple but promising experimental setup, along with discrete element simulations that successfully reproduced the different granule classes observed in the experiments and conclude the following:

1. Granulation of snow is highly temperature dependent with a snow temperature threshold at -1°C . Below this temperature no persistent granules were observed. If the snow temperature exceeded -1°C granulation occurred very fast and was most effective for new snow or decomposed forms close to 0°C .
2. Persistent granules can be further differentiated into moist or wet granules. These two (persistent) granule types showed significantly different mechanical properties upon collision.
3. Granulation is mostly relevant for snow with a temperature warmer than -1°C and therefore for warm or wet avalanches. At lower temperatures the potential for the formation of persistent granules is very low. Therefore, granular structures as often observed (at the surface) in the deposition zone of cold avalanches are more likely to be fragments of the released or eroded snow cover.
4. DEM Simulations allowed to better characterize the underlying processes of granulation by means of agglomeration and fragmentation propensity.
5. The presented modeling approach provides a first step toward more complex and real-scale modeling of flowing cohesive snow with varying properties.
6. A quantification to which extent granulation and thus the granule size distribution depends on snow temperature is possible.

To gain a better understanding and link the effect of the snow cover on flow dynamics, further interdisciplinary research is necessary. The main challenge will be to accurately define the linking processes between the microscopic (crystal) scale, e.g., sintering, the mesoscopic scale, e.g., energy dissipation during granule interaction, and the macroscopic scale, e.g., flow dynamics. To accurately model snow avalanches for different snow temperatures and consequently different flow dynamics [Vera *et al.*, 2012], it is necessary to reproduce the temperature-dependent granule size distribution as well as possible. Model calculations as shown in section 2.2 represent a first approach in this direction.

Acknowledgments

Document data are available on request by contacting Walter Steinkogler at (w.steinkogler@gmail.com). Funding for this research has been provided through the Interreg project STRADA by the following partners: Amt für Wald Graubünden, Etat du Valais, ARPA Lombardia, ARPA Piemonte, Valle d'Aosta, and Regione Lombardia. J. Gaume was supported by the Swiss Government Excellence Scholarship and is grateful to the State Secretariat for Education, Research and Innovation SERI of the Swiss Government. We thank the Editor Alexander Densmore, the Associate Editor and three anonymous reviewers for their valuable comments and remarks that helped us to improve our paper.

References

- Alexander, A. W., B. Chaudhuri, A. Faqih, F. J. Muzzio, C. Davies, and M. S. Tomassone (2006), Avalanching flow of cohesive powders, *Powder Technol.*, *164*(1), 13–21, doi:10.1016/j.powtec.2006.01.017.
- Andreotti, B., Y. Forterre, and O. Pouliquen (2013), *Granular media*, 1st ed., Cambridge Univ. Press, Cambridge, U. K., doi:10.1017/CBO9781139541008.
- Baroudi, D., B. Sovilla, and E. Thibert (2011), Effects of flow regime and sensor geometry on snow avalanche impact-pressure measurements, *J. Glaciol.*, *57*(202), 277–288, doi:10.3189/002214311796405988.
- Barrasso, D., and R. Ramachandran (2014), Multi-scale modeling of granulation processes: Bi-directional coupling of PBM with DEM via collision frequencies, *Chem. Eng. Res. Des.*, *93*, 304–317, doi:10.1016/j.cherd.2014.04.016.
- Bartelt, P., and B. W. McARDell (2009), Granulometric investigations of snow avalanches, *J. Glaciol.*, *55*(193), 829–833, doi:10.3189/002214309790152384.
- Bartelt, P., J. Glover, T. Feistl, Y. Bühler, and O. Buser (2012), Formation of levees and en-echelon shear planes during snow avalanche run-out, *J. Glaciol.*, *58*(211), 980–992, doi:10.3189/2012JoG11J011.
- Bazant, Z. P., G. Zi, and D. McClung (2003), Size effect law and fracture mechanics of the triggering of dry snow slab avalanches, *J. Geophys. Res.*, *108*(B2), 2119, doi:10.1029/2002JB001884.
- Boltachev, G. S., N. B. Volkov, E. A. Kochurin, A. L. Maximenko, M. B. Shtern, and E. G. Kirkova (2014), Macromechanical behavior of oxide nanopowders during compaction processes, *Comput. Phys.*, arXiv preprint arXiv:1409.6393.
- Brown, N. J. (2013), Discrete element modelling of cementitious materials, PhD thesis, The Univ. of Edinburgh, Scotland, U. K.
- Casassa, G., H. Narita, and N. Maeno (1991), Shear cell experiments of snow and ice friction, *J. Appl. Geophys.*, *69*(6), 3745–3756, doi:10.1063/1.348469.
- Chaudhuri, B., A. Mehrotra, F. J. Muzzio, and M. S. Tomassone (2006), Cohesive effects in powder mixing in a tumbling blender, *Powder Technol.*, *165*(2), 105–114, doi:10.1016/j.powtec.2006.04.001.
- Cheong, Y., M. Adams, A. Routh, M. Hounslow, and A. Salman (2005), The production of binderless granules and their mechanical characteristics, *Chem. Eng. Sci.*, *60*(14), 4045–4053, doi:10.1016/j.ces.2005.02.033.
- Cundall, P. A., and O. D. Strack (1979), A discrete numerical model for granular assemblies, *Geotechnique*, *29*(1), 47–65, doi:10.1680/geot.1979.29.1.47.

- da Cruz, F., S. Emam, M. Prochnow, J. -N. Roux, and F. Chevoir (2005), Rheophysics of dense granular materials: Discrete simulation of plane shear flows, *Phys. Rev. E*, *72*(2), 21,309, doi:10.1103/PhysRevE.72.021309.
- Dash, J. G., A. W. Rempel, and J. S. Wettlaufer (2006), The physics of premelted ice and its geophysical consequences, *Rev. Mod. Phys.*, *78*(3), 695–741, doi:10.1103/RevModPhys.78.695.
- De Biagi, V., B. Chiaia, and B. Frigo (2012), Fractal grain distribution in snow avalanche deposits, *J. Glaciol.*, *58*(208), 340–346, doi:10.3189/2012JoG11J119.
- Donahue, C. M., C. M. Hrenya, R. H. Davis, K. J. Nakagawa, A. P. Zelinskaya, and G. G. Joseph (2010), Stokes' cradle: Normal three-body collisions between wetted particles, *J. Fluid Mech.*, *650*, 479–504, doi:10.1017/S0022112009993715.
- Ennis, B. J., G. Tardos, and R. Pfeffer (1991), A microlevel-based characterization of granulation phenomena, *Powder Technol.*, *65*(1–3), 257–272, doi:10.1016/0032-5910(91)80189-P.
- Faug, T., R. Beguin, and B. Chanut (2009), Mean steady granular force on a wall overflowed by free-surface gravity-driven dense flows, *Phys. Rev. E*, *80*, 21,305, doi:10.1103/PhysRevE.80.021305.
- Fierz, C., R. Armstrong, Y. Durand, P. Etchevers, E. Greene, D. McClung, K. Nishimura, P. Satyawali, and S. Sokratov (2009), *The international classification for seasonal snow on the ground*, IHP-VII Technical Documents in Hydrology, IACS Contribution, UNESCO-IHP, Paris.
- Gauer, P., D. Issler, K. Lied, K. Kristensen, and F. Sandersen (2008), On snow avalanche flow regimes: Inferences from observations and measurements, *paper presented at International Snow Science Workshop ISSW 2008*, pp. 717–723, Whistler, Canada.
- Gaume, J., G. Chambon, and M. Naaim (2011), Quasistatic to inertial transition in granular materials and the role of fluctuations, *Phys. Rev. E*, *84*(5), 51,304, doi:10.1103/PhysRevE.84.051304.
- Gaume, J., G. Chambon, N. Eckert, and M. Naaim (2012), Relative influence of mechanical and meteorological factors on avalanche release depth distributions, *Geophys. Res. Lett.*, *39*, L12401, doi:10.1029/2012GL051917.
- Gaume, J., G. Chambon, N. Eckert, M. Naaim, and J. Schweizer (2015a), Influence of weak layer heterogeneity and slab properties on slab tensile failure propensity and avalanche release area, *Cryosphere*, *9*(2), 795–804, doi:10.5194/tc-9-795-2015.
- Gaume, J., A. van Herwijnen, G. Chambon, J. Schweizer, and K. W. Birkeland (2015b), Modeling of crack propagation in weak snowpack layers using the discrete element method, *Cryosphere Discuss.*, *9*, 609–653, doi:10.5194/tcd-9-609-2015.
- GDR MiDi (2004), On dense granular flows, *Eur. Phys. J. E*, *14*(4), 341–365, doi:10.1140/epje/i2003-10153-0.
- Hagenmüller, P., T. C. Theile, and M. Schneebeli (2014), Numerical simulation of microstructural damage and tensile strength of snow, *Geophys. Res. Lett.*, *41*, 86–89, doi:10.1002/2013GL058078.
- Hapgood, K., S. Iveson, J. Litster, and L. Liu (2007), Chapter 20 granulation rate processes, in *Handbook of Powder Technology*, vol. 11, edited by K. Hapgood et al., pp. 897–977, Elsevier, Amsterdam.
- Hornbaker, D. J., R. Albert, I. Albert, A. -L. Barabasi, and P. Schiffer (1997), What keeps sandcastles standing?, *Nature*, *387*(6635), 765–765.
- Iveson, S. M., J. D. Litster, K. Hapgood, and B. J. Ennis (2001), Nucleation, growth and breakage phenomena in agitated wet granulation processes: A review, *Powder Technol.*, *117*(1), 3–39, doi:10.1016/S0032-5910(01)00313-8.
- Jamieson, B., and C. Johnston (1990), In-situ tensile tests of snowpack layers, *J. Glaciol.*, *36*(122), 102–106.
- Jamieson, J., and C. Johnston (2001), Evaluation of the shear frame test for weak snowpack layers, *Ann. Glaciol.*, *32*(1), 59–69, doi:10.3189/172756401781819472.
- Kapur, P. C. (1971), The crushing and layering mechanism of granule growth, *Chem. Eng. Sci.*, *26*(7), 1093–1099, doi:10.1016/0009-2509(71)80023-4.
- Kern, M., P. Bartelt, and B. Sovilla (2010), Velocity profile inversion in dense avalanche flow, *Ann. Glaciol.*, *51*(54), 27–31, doi:10.3189/172756410791386643.
- Kobayashi, T., Y. Nohguchi, and K. Izumi (2000), Comparison of dry granulation and wet agglomeration of snow, *paper presented at the Fourth International Conference on Snow Engineering*, pp. 93–97, Trondheim, Norway.
- Kristensen, H., and T. Schaefer (1987), Granulation. A review on pharmaceutical wet-granulation, *Drug Dev. Ind. Pharm.*, *13*(4–5), 803–872, doi:10.3109/03639048709105217.
- Kroupa, M., M. Klejch, M. Vonka, and J. Kosek (2012), Discrete Element Modeling (DEM) of agglomeration of polymer particles, *Procedia Eng.*, *42*, 58–69, doi:10.1016/j.proeng.2012.07.395.
- Louge, M. Y., C. S. Carroll, and B. Turnbull (2011), Role of pore pressure gradients in sustaining frontal particle entrainment in eruption currents: The case of powder snow avalanches, *J. Geophys. Res.*, *116*, F04030, doi:10.1029/2011JF002065.
- McClung, D. (2009), Dimensions of dry snow slab avalanches from field measurements, *J. Geophys. Res.*, *114*, F01006, doi:10.1029/2007JF000941.
- Mellmann, J. (2001), The transverse motion of solids in rotating cylinders—Forms of motion and transition behavior, *Powder Technol.*, *118*(3), 251–270, doi:10.1016/S0032-5910(00)00402-2.
- Mellor, M. (1974), *A Review of Basic Snow Mechanics*, US Army Cold Regions Research and Engineering Lab., Hanover.
- Mishra, B., and C. Thornton (2001), Impact breakage of particle agglomerates, *Int. J. Miner. Process.*, *61*(4), 225–239, doi:10.1016/S0301-7516(00)00065-X.
- Mitarai, N., and F. Nori (2006), Wet granular materials, *Adv. Phys.*, *55*(1–2), 1–45, doi:10.1080/00018730600626065.
- Moro, F., T. Faug, H. Bellot, and F. Ousset (2010), Large mobility of dry snow avalanches: Insights from small-scale laboratory tests on granular avalanches of bidisperse materials, *Cold Reg. Sci. Technol.*, *62*(1), 55–66, doi:10.1016/j.coldregions.2010.02.011.
- Naaim, M., Y. Durand, N. Eckert, and G. Chambon (2013), Dense avalanche friction coefficients: Influence of physical properties of snow, *J. Glaciol.*, *59*(216), 771–782, doi:10.3189/2013JoG12J205.
- Nohguchi, Y., T. Kobayashi, K. Iwanami, K. Nishimura, and A. Sato (1997), Granulation of snow, *paper presented at 3rd International Conference of Snow Engineering*, pp. 167–170, Sendai, Japan.
- Nowak, S., A. Samadani, and A. Kudrolli (2005), Maximum angle of stability of a wet granular pile, *Nature Phys.*, *1*(1), 50–52, doi:10.1038/nphys106.
- Ouchiyama, N., and T. Tanaka (1975), The probability of coalescence in granulation kinetics, *Ind. Eng. Chem., Process Des. Dev.*, *14*(3), 286–289, doi:10.1021/i260055a016.
- Patwa, A., R. Ambrose, H. Dogan, and M. Casada (2014), Wheat mill stream properties for discrete element method modeling, *Trans. ASABE*, *57*(3), 891–899.
- Phillips, J., A. Hogg, R. Kerswell, and N. Thomas (2006), Enhanced mobility of granular mixtures of fine and coarse particles, *Earth Planet. Sci. Lett.*, *246*(3), 466–480, doi:10.1016/j.epsl.2006.04.007.
- Pietsch, W. (2003), An interdisciplinary approach to size enlargement by agglomeration, *Powder Technol.*, *130*(1), 8–13, doi:10.1016/S0032-5910(02)00218-8.
- Podolskiy, E. A., M. Barbero, F. Barpi, G. Chambon, M. Borri-Brunetto, O. Pallara, B. Frigo, B. Chiaia, and M. Naaim (2014), Healing of snow surface-to-surface contacts by isothermal sintering, *Cryosphere*, *8*(5), 1651–1659, doi:10.5194/tc-8-1651-2014.

- Pouliquen, O. (1999), Scaling laws in granular flows down rough inclined planes, *Phys. Fluids*, *11*(3), 542–548, doi:10.1063/1.869928.
- Pruppacher, H., and J. Klett (1997), *Microphysics of Clouds and Precipitation*, Atmospheric and Oceanographic Sciences Library, Springer, Netherlands, doi:10.1080/02786829808965531.
- Pudasaini, S. P., and S. A. Miller (2013), The hypermobility of huge landslides and avalanches, *Eng. Geol.*, *157*(0), 124–132, doi:10.1016/j.enggeo.2013.01.012.
- Radjai, F., et al. (2011), *Discrete-element Modeling of Granular Materials*, Wiley, Hoboken.
- Rastello, M., and E. Hopfinger (2004), Sediment-entraining suspension clouds: A model of powder-snow avalanches, *J. Fluid Mech.*, *509*, 181–206, doi:10.1017/S0022112004009322.
- Reed, J. S. (1995), *Principles of Ceramics Processing*, 2nd ed., Wiley, Hoboken.
- Reinhold, A., and H. Briesen (2012), Numerical behavior of a multiscale aggregation model-coupling population balances and discrete element models, *Chem. Eng. Sci.*, *70*, 165–175, doi:10.1016/j.ces.2011.06.041.
- Roche, O., M. Attali, A. Mangeney, and A. Lucas (2011), On the run-out distance of geophysical gravitational flows: Insight from fluidized granular collapse experiments, *Earth Planet. Sci. Lett.*, *311*(34), 375–385, doi:10.1016/j.epsl.2011.09.023.
- Rognon, P., J.-N. Roux, M. Naaim, and F. Chevoir (2008a), Dense flows of cohesive granular materials, *J. Fluid Mech.*, *596*, 21–47, doi:10.1017/S0022112007009329.
- Rognon, P., F. Chevoir, H. Bellot, F. Ousset, M. Naaim, and P. Coussot (2008b), Rheology of dense snow flows: Inferences from steady state chute-flow experiments, *J. Rheol.*, *52*(3), 729–748, doi:10.1122/1.2897609.
- Roux, J.-N., and G. Combe (2002), Quasistatic rheology and the origins of strain, *C. R. Phys.*, *3*(2), 131–140, doi:10.1016/S1631-0705(02)01306-3.
- Sarkar, A., and C. Wassgren (2010), Continuous blending of cohesive granular material, *Chem. Eng. Sci.*, *65*(21), 5687–5698, doi:10.1016/j.ces.2010.04.011.
- Sarkar, A., and C. R. Wassgren (2009), Simulation of a continuous granular mixer: Effect of operating conditions on flow and mixing, *Chem. Eng. Sci.*, *64*(11), 2672–2682, doi:10.1016/j.ces.2009.02.011.
- Scapozza, C., and P. Bartelt (2003), Triaxial tests on snow at low strain rate. Part II. Constitutive behaviour, *J. Glaciol.*, *49*(164), 91–101, doi:10.3189/172756503781830890.
- Schaefer, M., and L. Bugnion (2013), Velocity profile variations in granular flows with changing boundary conditions: Insights from experiments, *Phys. Fluids*, *25*(6), 63,303, doi:10.1063/1.4810973.
- Schiffer, P. (2005), Granular physics: A bridge to sandpile stability, *Nature Phys.*, *1*(1), 21–22, doi:10.1038/nphys129.
- Schubert, H. (1977), Tensile strength and capillary pressure of moist agglomerates, *Agglomeration*, *77*, 144–155.
- Sigrist, C. (2006), Measurement of fracture mechanical properties of snow and application to dry snow slab avalanche release, PhD thesis, Univ. of Bern, Switzerland.
- Sigrist, C., J. Schweizer, H.-J. Schindler, and J. Dual (2005), On size and shape effects in snow fracture toughness measurements, *Cold Reg. Sci. Technol.*, *43*(1), 24–35, doi:10.1016/j.coldregions.2005.05.001.
- Siirä, S. M., O. Antikainen, J. Heinämäki, and J. Yliruusi (2011), 3D simulation of internal tablet strength during tableting, *AAPS PharmSciTech*, *12*(2), 593–603, doi:10.1208/s12249-011-9623-0.
- Sovilla, B., and P. Bartelt (2002), Observations and modelling of snow avalanche entrainment, *Nat. Hazards Earth Syst. Sci.*, *2*(3/4), 169–179, doi:10.5194/nhess-2-169-2002.
- Sovilla, B., S. Margreth, and P. Bartelt (2007), On snow entrainment in avalanche dynamics calculations, *Cold Reg. Sci. Technol.*, *47*(1–2), 69–79, doi:10.1016/j.coldregions.2006.08.012.
- Sovilla, B., M. Schaer, M. Kern, and P. Bartelt (2008), Impact pressures and flow regimes in dense snow avalanches observed at the Vallée de la Sionne test site, *J. Geophys. Res.*, *113*, F01010, doi:10.1029/2006JF000688.
- Sovilla, B., M. Kern, and M. Schaer (2010), Slow drag in wet-snow avalanche flow, *J. Glaciol.*, *56*(198), 587–592, doi:10.3189/002214310793146287.
- Steinkogler, W., B. Sovilla, and M. Lehning (2014a), Influence of snow cover properties on avalanche dynamics, *Cold Reg. Sci. Technol.*, *97*, 121–131, doi:10.1016/j.coldregions.2013.10.002.
- Steinkogler, W., B. Sovilla, and M. Lehning (2014b), Thermal energy in dry snow avalanches, *Cryosphere Discuss.*, *8*(6), 5793–5824, doi:10.5194/tcd-8-5793-2014.
- Subero, J., and M. Ghadiri (2001), Breakage patterns of agglomerates, *Powder Technol.*, *120*(3), 232–243, doi:10.1016/S0032-5910(01)00276-5.
- Szabo, D., and M. Schneebeli (2007), Subsecond sintering of ice, *Appl. Phys. Lett.*, *151*, 916–151,916(15), doi:10.1063/1.2721391.
- Tegzes, P., T. Vicsek, and P. Schiffer (2003), Development of correlations in the dynamics of wet granular avalanches, *Phys. Rev. E.*, *67*(5), 51,303, doi:10.1103/PhysRevE.67.051303.
- Vera, C., T. Feistl, W. Steinkogler, O. Buser, and P. Bartelt (2012), Thermal temperature in avalanche flow, paper presented at International Snow Science Workshop ISSW 2012, pp. 32–37, Anchorage, Alaska.
- Vervaeke, C., and J. P. Remon (2005), Continuous granulation in the pharmaceutical industry, *Chem. Eng. Sci.*, *60*(14), 3949–3957, doi:10.1016/j.ces.2005.02.028.
- Von Smoluchowski, M. (1917), Versuch einer mathematischen Theorie der Koagulationskinetik kolloidaler Lösungen, *Z. Phys. Chem.*, *92*(2), 129–168.
- Walker, G. M. (2007), Chapter 4 drum granulation processes, in *Granulation*, vol. 11, edited by G. M. Walker, pp. 219–254, Elsevier, Amsterdam.